Mitigation for turbulence effects in a 40-Gbit/s orbital-angular-momentum-multiplexed free-space optical link between a ground station and a retro-reflecting UAV using MIMO equalization

LONG LI,[1,*] RUNZHOU ZHANG,[1] PEICHENG LIAO,[1] YINWEN CAO,[1] HAOQIAN SONG,[1] YIFAN ZHAO,[1,2] JING DU,[1] ZHE ZHAO,[1] CONG LIU,[1] KAI PANG,[1] HAO SONG,[1] AHMED ALMAIMAN[1,3] DMITRY STARODUBOV,[1] BRITTANY LYNN,[4] ROBERT BOCK,[5] MOSHE TUR,[6] , ANDREAS, F. MOLISCH,[1] ALAN E. WILLNER,[1]

[1]*Department of Electrical Engineering, University of Southern California, Los Angeles, CA 90089, USA*
[2]*School of Optical and Electronic Information, Huazhong University of Science and Technology, Wuhan 430074, China*
[3]*King Saud University, Riyadh, SAUDI ARABIA*
[4]*Space & Naval Warfare Systems Center, Pacific, San Diego, CA 92152, USA*
[5]*R-DEX System, Marietta, GA 30068, USA*
[6]*School of Electrical Engineering, Tel Aviv University, Ramat Aviv 69978, Israel*
**Corresponding author: longl@usc.edu*

Received XX Month XXXX; revised XX Month, XXXX; accepted XX Month XXXX; posted XX Month XXXX (Doc. ID XXXXX); published XX Month XXXX

We experimentally demonstrate turbulence effect mitigation in a 100-m round-trip orbital-angular-momentum (OAM)-multiplexed free-space optical (FSO) communication link between a ground transmitter and a ground receiver via a retro-reflecting hovering unmanned-aerial-vehicle (UAV) using multiple-input-multiple-output (MIMO) equalization. In our demonstration, two OAM beams at 1550 nm are transmitted to the UAV through emulated atmospheric turbulence, each carrying a 20-Gbit/s signal. 2×2 MIMO equalization is used to mitigate turbulence-induced crosstalk between the two OAM channels. Bit error rates (BERs) below the 7% overhead forward error correction (FEC) limit of 3.8×10^{-3} are achieved for both channels. © **2019 Optical Society of America**

OCIS codes: *(060.2605) Free-space optical communications; (050.4865) Optical vortices.*

http://dx.doi.org/10.1364/OL.99.099999

The communications capacity needs of manned and unmanned aerial platforms as well as their ground stations have kept increasing over recent years [1]. Compared to radio frequency links, FSO communications can potentially provide higher link capacity and lower probability of detection due to its higher optical carrier frequency and its lower diffraction properties [2,3].

Moreover, space-division-multiplexing (SDM) has gained interest to further increase link capacity in FSO communications, in which multiple independent data-carrying beams are transmitted over the same spatial medium [4,5]. One subset of SDM is mode-division-multiplexing (MDM), in which each beam uses a different mode from a modal basis set [4,5]. One example of MDM is multiplexing multiple OAM beams [6-7]. An OAM-carrying beam has a phase-front "twisting" in a helical fashion and its OAM order is defined by the number of 2π phase shifts in the azimuthal direction and represented by an integer ℓ [8]. OAM beams with different orders are orthogonal with each other, such that multiple beams can be (de)multiplexed with low inherent crosstalk [9].

In general, atmospheric turbulence is one of the key challenges for FSO communications that degrade link performance [10]. The level of turbulence strength is characterized by the atmospheric structure constant C_n^2, typical values of which vary from 10^{-17} $m^{-2/3}$ (weak) to 10^{-12} $m^{-2/3}$ (strong) [11,12].This issue is of greater concern for OAM-multiplexed links, since turbulence can cause phase distortions to OAM beams and increased crosstalk among different OAM channels [13,14].

There have been reports of turbulence effect mitigation for OAM-multiplexed FSO links between fixed transmitters and receivers using: (i) adaptive optics with a wavefront sensor to detect the beam profile and then correct the phase distortion in

optical domain [15]; and (ii) MIMO digital signal processing (DSP) algorithm to mitigate OAM channel crosstalk: such electronic approach does not require additional optical elements for sensing and correcting the distortions [16]. Moreover, there have been reports of using MIMO equalization to mitigate turbulence effects in an OAM-multiplexed link in a lab environment either in free-space or through underwater over roughly a 1-m distance [16,17]. Recently, a 100-m round-trip OAM-multiplexed link between a ground station and a retro-reflecting flying UAV has been reported [18], but the turbulence issue was not addressed in that work.

In this Letter, we experimentally demonstrate MIMO equalization to mitigate emulated turbulence in a 40-Gbit/s retro-reflected FSO link multiplexing 2 OAM modes between a ground transmitter and a ground receiver, connected via a flying retro-reflecting UAV over 100-m round-trip distance [19]. The receiver is co-located with the transmitter on the ground station. A rotatable phase plate with a pseudo-random phase distribution, obeying Kolmogorov spectrum statistics is used at the transmitter to emulate atmospheric turbulence [14]. Results indicate that MIMO equalization could help mitigate the crosstalk caused by turbulence, and improve both error vector magnitude (EVM) and BER of the signal in an OAM-multiplexed link for flying platforms. In our experiment, MIMO equalization helps achieve BER values mostly below 3.8×10^{-3} under the emulated turbulence.

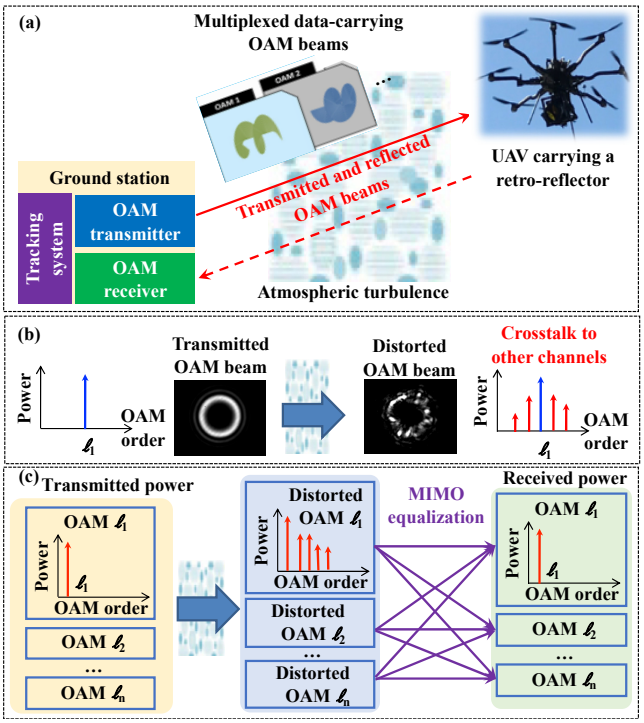

Fig. 1. Concept of (a) an OAM-multiplexed FSO communication link between a ground station and a retro-reflecting UAV through atmospheric turbulence; (b) an OAM beam distorted by turbulence; and (c) mitigation for turbulence effect in an OAM-multiplexed link using multiple-input-multiple-output (MIMO) equalization.

Figure 1(a) shows the concept of an OAM-multiplexed FSO link between a ground station and a retro-reflecting UAV. Multiple independent data-carrying OAM beams are multiplexed and transmitted from the ground station to the UAV, and retro-reflected back to the same ground station. Due to atmospheric turbulence, the OAM beams may be distorted during their free-space propagation, such that signal power on each particular OAM mode may be coupled to its neighbouring modes, as shown in Fig. 1(b). Therefore, the received signal at a particular mode may also contain crosstalk from its neighbours. MIMO equalization could help reduce crosstalk among channels by applying the inverse channel matrix to the received signals, thus mitigating performance degradation in a coherent optical communications link, as shown in Fig. 1(c) [16,17].

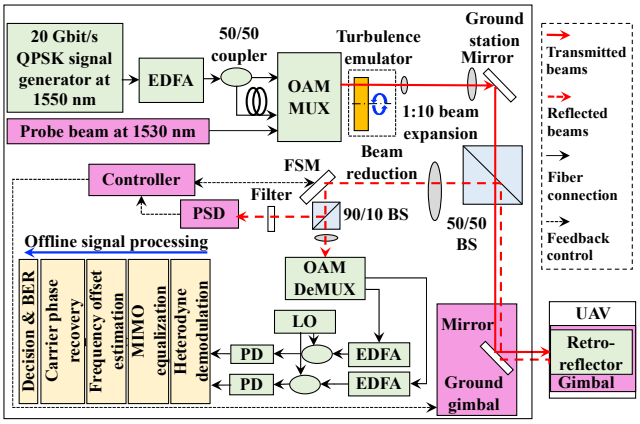

Fig. 2. Experimental setup. BS: beamsplitter; DeMUX: demultiplexer; EDFA: erbium-doped fiber amplifier; FSM: fast steering mirror; LO: local oscillator; MUX: multiplexer; PD: photodetector; PSD: position sensitive detector; QPSK: quadrature phase-shift keying.

The experimental setup is shown in Fig. 2. During the measurement, the UAV is either on the ground, hovering, or moving at a maximum speed of ~0.1 m/s, ~50-m away from the ground station. A 20-Gbit/s quadrature phase-shift keying (QPSK) signal at 1550 nm is generated and split into two branches. One branch is relatively delayed using a ~10-m single-mode fiber to decorrelate the data sequences. The two branches are fed to two input ports of a custom-designed OAM generator/multiplexer, generating multiplexed OAM beams [20]. Another 1530-nm beacon for beam tracking is sent to the $\ell = 0$ input port of the OAM multiplexer. These co-axially propagating beams then pass through a thin phase plate mounted on a rotation stage. This phase plate is designed to generate a pseudo-random phase distribution obeying the Kolmogorov spectrum statistics with a Fried parameter r_0 of 1 mm [14]. Then the beams are expanded and propagate to the gimbal-mounted retro-reflector carried by the UAV. The beam diameters after expansion are ~ 6.0 cm and ~ 4.2 cm for OAM -3 and +1 beams. The retro-reflector reverses the beam's OAM order from $+\ell$ to $-\ell$. After the tenfold beam expansion, the effective r_0 is ~ 10 mm, which corresponds to atmospheric structure constant $C_n^2 \sim 3\times10^{-12}$ $m^{-2/3}$ (strong) for emulated 100-m propagation distance [11], based on the relation $r_0 = [0.423k^2C_n^2L]^{-3/5}$ where k and L are wave number and emulated propagation length, respectively [14]. At the receiver and after diameter reduction, the beams are coupled into the OAM demultiplexer for heterodyne detection and MIMO equalization based on a constant modulus algorithm (CMA): multiple signals are received simultaneously from different OAM modes and then the CMA utilized all the signals to mitigate channel crosstalk by applying a linear equalizer [16]. In our demonstration, the signal at the transmitter and the local oscillator (LO) at the receiver are co-

located at the same ground station, but originated from two different laser sources. The coherence between the LO and signal is achieved by digital signal processing algorithms in the coherent receiver, such as frequency offset and phase noise recovery [16]. A two-stage beam tracking system is used in the receiver [19]: A coarse tracking system controls the gimbal to make the OAM beams pointing to the UAV, and a fine tracking system keeps the reflected beams hit the centre of the OAM demultiplexer.

First, we measure the Rytov variance σ^2 with and without placing the turbulence phase plate in the link. Such a variance characterizes the received power scintillation of this link induced by the turbulence effects, and it can be expressed as $\sigma^2 = 0.56k^{7/6}C_n^2 d(L/4)^{5/6}$ where d and L are the thickness of phase plate and the link distance, respectively [14]. Typically, $\sigma^2 < 1$, $\sigma^2 \sim 1$, and $\sigma^2 > 1$ correspond to weak, moderate, and strong power scintillations, respectively [11]. The retro-reflector carried by the UAV is placed on the ground ~50 m away from the transmitter/ receiver. A ~5-cm diameter 1550-nm Gaussian probe beam propagates from the transmitter to the retro-reflector and back to the receiver. At the receiver, a ~1-mm diameter point detector is used to record the received power over a 10-minute period. Figs. 3(a) and 3(b) show the received power distributions when the turbulence plate is rotating at 40 round/minute or not presented in the link, and σ^2 is found to be 0.11 and 0.003, respectively. We note that the Rytov variance depends on both the atmospheric structure constant C_n^2 and the link distance L [14]. Although our phase plate emulates strong turbulence strength ($C_n^2 \sim 3 \times 10^{-12}$ $m^{-2/3}$), the power scintillation of this link is weak since the link distance is limited to 100 m.

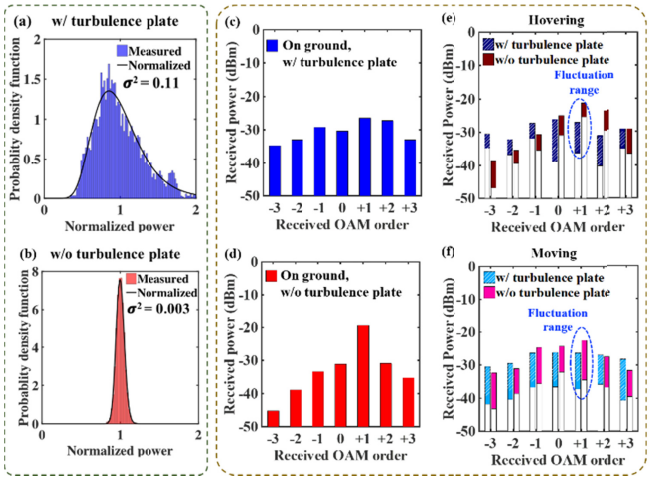

Fig. 3. Measured power distribution when the turbulence emulator is (a) placed in the link and rotating at 40 round/minute and (b) not placed in the link. A ~5-cm diameter 1550-nm Gaussian probe beam is transmitted over ~100 m roundtrip, and a ~1-mm diameter point detector is used at the receiver; Measured OAM spectrum when OAM +1 beam is transmitted when the UAV is (c) static on the ground with turbulence plate, (d) static on the ground without the turbulence phase plate, (e) hovering in the air, and (f) moving at a maximum speed of 0.1 m/s. (e) and (f) are measured in a 60-second period.

The turbulence strength is characterized by the Fried parameter r0, which is fixed as 0.1 mm. However, the distortion effects induced by the emulated is characterized by the ratio of the OAM beam size D and Fried parameter r_0 [21]. Therefore, different-sized OAM beams may experience different distortion effects under the same turbulence strength. In our experiment, D/r_0 for OAM -3 and +1 beams are measured to be ~6.0 and ~4.2, respectively, corresponding to strong distortion effects [21]. Figures 3(c)~3(f) shows the measured OAM spectrum when only the OAM +1 beam is transmitted under various flight conditions with and without placing the turbulence phase plate. In Figs. 3(c) and 3(d), the UAV is static on the ground, ~50-m away from the ground station; In Figs. 3(e) and 3(f), the UAV is hovering or moving at a maximum speed of ~0.1 m/s, ~50-m away from the ground station and ~5-m above the ground. When the UAV is hovering or moving, the received power on different modes fluctuates, due to both imperfect beam tracking and turbulence effects [18]. The shaded portion of each bar in Figs. 3(e) and 4(f) represents the fluctuation range of received power. In this measurement, the turbulence phase plate is fixed at a random angle without rotating when placed in the link, emulating a random turbulence realization. Results show that turbulence increases the channel crosstalk under all flight conditions.

Figure 4 shows the instantaneous power and crosstalk for OAM +1 and -3 when both beams are simultaneously transmitted under 12 different turbulence realizations (i.e., different randomly chosen angles of the turbulence phase plate). With the phase plate fixed, such emulated turbulence effects induce weak power scintillation, which follows a probability density function with the same Rytov variance of 0.11 as measured in Fig. 3(a). The atmospheric structure constant C_n^2 is still $\sim 3 \times 10^{-12}$ $m^{-2/3}$, which corresponds to strong turbulence strength [12]. We note that in each realization, the phase plate would randomly affect the OAM beams, resulting in different levels of distortions. Here, crosstalk of a specific channels is defined as the power received from other unwanted modes over the power received from the desired mode. The UAV is hovering ~50-m away from the ground station and ~5-m above the ground. Results show that the OAM -3 channel generally has lower power and suffers from higher crosstalk compared with the OAM +1 channel. This may be due to the fact that, with the same beam waist w_0, the size of an OAM beam is proportional to $\sqrt{|\ell| + 1}$ [22]. Therefore, the D/r_0 for OAM -3 is larger than that of OAM +1, leading to a larger turbulence-induced distortion for OAM -3 beam.

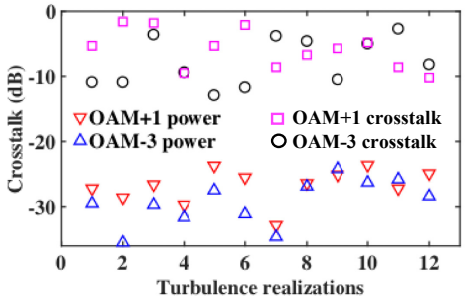

Fig. 4. Measured power and crosstalk for OAM+1 and -3 when both beams are transmitted under 12 different turbulence realizations. The UAV is hovering ~50-m away, ~5-m above the ground.

Figure 5 shows the BER measurements when both OAM -3 and +1 channels are transmitted, each carrying a 20-Gbit/s QPSK signal. Figure 5(a) shows BERs for the OAM -3 as functions of transmitted power when the UAV is static on the ground or hovering ~50-m

away, with and without the turbulence phase plate. No MIMO equalization has been used. It is shown that the measured BER curve of OAM -3 without MIMO equalization exhibits a severe error floor due to the inter-channel crosstalk. Furthermore, Fig. 5(b) shows BERs for both channels as functions of transmitted power when the UAV is hovering ~50-m away with phase plate fixed at a random angle. We observe that the BERs dramatically decrease to below the 7% overhead FEC limit of 3.8×10^{-3} for all channels after MIMO equalization. The received QPSK constellation diagrams and corresponding EVMs for both channels are shown in Fig. 5(c). The transmitted power for both channels is 10 dBm. We then rotate the phase plate randomly to different angles to test the system under various turbulence realizations. Fig. 5(d) shows the measured BERs for both channels under 12 different turbulence realizations. Note that the results in Fig. 4 and Fig. 5(d) are measured in two different runs, and the turbulence realizations are different. For each realization, the transmitted power for each channel is 10 dBm. We observe that the BER improvement of using MIMO equalization varies for different realizations, but such BERs are mostly kept below 3.8×10^{-3} FEC limit for both channels.

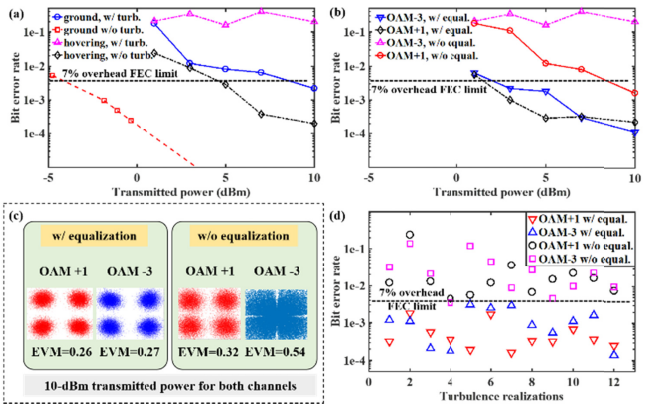

Fig. 5. Measured BERs as functions of transmitted power when OAM +1 and OAM -3 are simultaneously transmitted, each carrying a 20-Gbit/s quadrature phase-shift keying (QPSK) signal: (a) OAM -3 channel without MIMO equalization; (b) both channels with and without MIMO equalization; (c) Recovered QPSK constellations for both channels with and without MIMO equalization; (d) both channels with and without MIMO equalization under 12 turbulence realizations. The UAV is hovering ~ 50-m away, ~5-m above the ground.

We note that, with longer transmission distances (> 100 m) in turbulent atmosphere, beam diffraction effects might also affect link performance including: (i) extra link loss due to limited aperture size [23]; (ii) mode-dependent loss due to mode-dependent divergence effects [22] ; and (iii) stronger turbulence-induced distortion effects caused by larger size of the diffracted OAM beam [21]. To scale our experimental results for longer transmission distance, one may need to consider [23]: (i) the design of the transmitted beam size and receiver aperture size to reduce link loss; and (ii) the selection of OAM orders and OAM spacings to reduce channel crosstalk. In summary, we experimentally demonstrated the use of MIMO equalization to mitigate emulated turbulence effects in a 2-channel 20-Gbit/s OAM-multiplexed FSO link between ground stations via a UAV over a 100-m round-trip distance. The results show that MIMO equalization can mitigate channel crosstalk and help achieve BER performance below the 7% FEC limit.

Funding. Air Force Office of Scientific Research (AFOSR) (FA9550-16-C-0008); National Science Foundation (NSF) (ECCS-1509965, IIP-1622777); Vannevar Bush Faculty Fellowship program sponsored by the Basic Research Office of the Assistant Secretary of Defense (ASD) for Research and Engineering (R&E) and funded by the Office of Naval Research (ONR) (N0014-16-1-2813).

References

1. W. S. Rabinovich, C. I. Moore, R. Mahon, P. G. Goetz, H. R. Burris, M. S. Ferraro, J. L. Murphy, L. M. Thomas, G. C. Gilbreath, M. Vilcheck, and M. R. Suite, Appl. Opt. **54**, F189 (2015).
2. A. Kaadan, H. Refai, and P. G. LoPresti, J. Lightw. Techno. **32**, 4183 (2014).
3. A. Glenn, IEEE Comm. Magazine **21**, 26 (1983).
4. G. Gibson, J. Courtial, M. J. Padgett, M. Vasnetsov, V. Pas'ko, S. M. Barnett, and S. Franke-Arnold, Opt. Express **12**, 5448 (2004).
5. D. Richardson, J. Fini, and L. E. Nelson, Nat. Photonics **7**, 354 (2013).
6. A. Trichili, C. Rosales-Guzmán, A. Dudley, B. Ndagano, A. B. Salem, M. Zghal, and A. Forbes, Sci. Rep. **6**, 27674 (2016).
7. J. Wang, J.-Y. Yang, I. Fazal, N. Ahmed, Y. Yan, H. Huang, Y. Ren, Y. Yue, S. Dolinar, M. Tur, and A. E. Willner, Nat. Photonics **6**, 488 (2012).
8. L. Allen, M. W. Beijersbergen, R. J. C. Spreeuw, and J. P. Woerdman, Phys. Rev. A **45**, 8185 (1992).
9. A. Yao, and M. Padgett, Adv. Opt. Photonics **3**, 161 (2011).
10. Z. Qu, and I. Djordjevic, Opt. Lett. **41**, 3285 (2016).
11. L. C. Andrews, R. L. Phillips, and A. R. Weeks, Waves in Random Media **7**, 229 **(**1997).
12. S. M. Augustine, N. Chetty, Atmósfera **27**, 385 (2014).
13. B. Rodenburg, M. Mirhosseini, M. Malik, O. S. Magaña-Loaiza, M. Yanakas, L. Maher, N. K. Steinhoff, G. A. Tyler, and R. W. Boyd, New J. Phys. **16**, 033020 (2014).
14. Y. Ren, H. Huang, G. Xie, N. Ahmed, Y. Yan, B. I. Erkmen, N. Chandrasekaran, M. P. J. Lavery, N. K. Steinhoff, M. Tur, S. Dolinar, M. Neifeld, M. J. Padgett, R. W. Boyd, J. H. Shapiro, and A. E. Willner, Opt. Lett. **38**, 4062 (2013).
15. Y. Ren, G. Xie, H. Huang, N. Ahmed, Y. Yan, L. Li, C. Bao, M. P. J. Lavery, M. Tur, M. A. Neifeld, R. W. Boyd, J. H. Shapiro, and A. E. Willner, Optica **1**, 376 **(**2014).
16. H. Huang, Y. Cao, G. Xie, Y. Ren, Y. Yan, C. Bao, N. Ahmed, M. A. Neifeld, S. J. Dolinar, and A. E. Willner, Opt. Lett. **39**, 4360 (2014).
17. Y. Ren, L. Li, Z. Wang, S. M. Kamali, E. Arbabi, A. Arbabi, Z. Zhao, G. Xie, Y. Cao, N. Ahmed, Y. Yan, C. Liu, A. J. Willner, S. Ashrafi, M. Tur, A. Faraon, and A. E. Willner, Sci. Rep. **6**, 33306 (2016).
18. L. Li, R. Zhang, Z. Zhao, G. Xie, P. Liao, K. Pang, H. Song, C. Liu, Y. Ren, G. Labroille, P. Jian, D. Starodubov, R. Bock, M. Tur, and A. E. Willner, Sci. Rep. **7**, 17427 (2017).
19. L. Li, R. Zhang, P. Liao, Y. Cao, H. Song, Y. Zhao, J. Du, Z. Zhao, C. Liu, K. Pang, H. Song, D. Starodubov, B. Lynn, R. Bock, M. Tur, A. F. Molisch, and A. E. Willner, In 2018 *European Conference on Optical Communication (ECOC)*, Th2.33 (2018).
20. G. Labroille, B. Denolle, P. Jian, P. Genevaux, N. Treps, and J.-F. Morizur, Opt. Express **22**, 15599 (2014).
21. B. Rodenburg, M. P. J. Lavery, M. Malik, M. N. O'Sullivan, M. Mirhosseini, D. J. Robertson, M. Padgett, and R. W. Boyd, Opt. Lett. **37**, 3735 (2012).
22. M. J. Padgett, F. M. Miatto, M. P. J. Lavery, A. Zeilinger, and R. W. Boyd, New J. Phys. **17**, 023011 (2015).
23. G. Xie, L. Li, Y. Ren, H. Huang, Y. Yan, N. Ahmed, Z. Zhao, M. P. J. Lavery, N. Ashrafi, S. Ashrafi, R. Bock, M. Tur, A. F. Molisch, and A. E. Willner, Optica **2**, 357 (2015).

Full References

1. W. S. Rabinovich, C. I. Moore, R. Mahon, P. G. Goetz, H. R. Burris, M. S. Ferraro, J. L. Murphy, L. M. Thomas, G. C. Gilbreath, M. Vilcheck, and M. R. Suite, "Free-space optical communications research and demonstrations at the U.S. Naval Research Laboratory," Applied Optics **54**, F189 (2015).
2. A. Kaadan, H. Refai, and P. G. LoPresti, "Multielement FSO transceivers alignment for inter-UAV communications," Journal of Lightwave Technology **32**, 4183 (2014).
3. A. Glenn, "Low probability of intercept," IEEE Communications Magazine **21**, 26 (1983).
4. G. Gibson, J. Courtial, M. J. Padgett, M. Vasnetsov, V. Pas'ko, S. M. Barnett, and S. Franke-Arnold, "Free-space information transfer using light beams carrying orbital angular momentum," Optics Express **12**, 5448 (2004).
5. D. Richardson, J. Fini, and L. E. Nelson, "Space-division multiplexing in optical fibres," Nature Photonics **7**, 354 (2013).
6. A. Trichili, C. Rosales-Guzmán, A. Dudley, B. Ndagano, A. B. Salem, M. Zghal, and A. Forbes, "Optical communication beyond orbital angular momentum," Scientific Reports **6**, 27674 (2016).
7. J. Wang, J.-Y. Yang, I. Fazal, N. Ahmed, Y. Yan, H. Huang, Y. Ren, Y. Yue, S. Dolinar, M. Tur, and A. E. Willner, "Terabit free-space data transmission employing orbital angular momentum multiplexing," Nature Photonics **6**, 488 (2012).
8. L. Allen, M. W. Beijersbergen, R. J. C. Spreeuw, and J. P. Woerdman, "Orbital angular momentum of light and the transformation of Laguerre-Gaussian laser modes," Physical Review A **45**, 8185 (1992).
9. A. Yao, M. Padgett, "Orbital angular momentum: origins, behavior and applications," Advances in Optics and Photonics **3**, 161 (2011).
10. Z. Qu, and I. Djordjevic, "500 Gb/s free-space optical transmission over strong atmospheric turbulence channels," Optics Letters **41**, 3285 (2016).
11. L. C. Andrews, R. L. Phillips, and A. R. Weeks, "Propagation of a Gaussian-beam wave through a random phase screen," Waves in Random Media 7, 229–244 (1997).
12. S. M. Augustine, and N. Chetty, "Experimental verification of the turbulent effects on laser beam propagation in space" Atmósfera 27, 385-401 (2014).
13. B. Rodenburg, M. Mirhosseini, M. Malik, O. S. Magaña-Loaiza, M. Yanakas, L. Maher, N. K. Steinhoff, G. A. Tyler, and R. W. Boyd, "Simulating thick atmospheric turbulence in the lab with application to orbital angular momentum communication," New Journal of Physics **16**, 033020 (2014).
14. Y. Ren, H. Huang, G. Xie, N. Ahmed, Y. Yan, B. I. Erkmen, N. Chandrasekaran, M. P. J. Lavery, N. K. Steinhoff, M. Tur, S. Dolinar, M. Neifeld, M. J. Padgett, R. W. Boyd, J. H. Shapiro, and A. E. Willner, "Atmospheric turbulence effects on the performance of a free space optical link employing orbital angular momentum multiplexing," Optics Letters **38**, 4062-4065 (2013).
15. Y. Ren, G. Xie, H. Huang, N. Ahmed, Y. Yan, L. Li, C. Bao, M. P. J. Lavery, M. Tur, M. A. Neifeld, R. W. Boyd, J. H. Shapiro, and A. E. Willner, "Adaptive-optics-based simultaneous pre- and post-turbulence compensation of multiple orbital-angular-momentum beams in a bidirectional free-space optical link," Optica **1**, 376-382 (2014).
16. H. Huang, Y. Cao, G. Xie, Y. Ren, Y. Yan, C. Bao, N. Ahmed, M. A. Neifeld, S. J. Dolinar, and A. E. Willner, "Crosstalk mitigation in a free-space orbital angular momentum multiplexed communication link using 4x4 MIMO equalization," Optics Letters **39**, 4360-4363 (2014).
17. Y. Ren, L. Li, Z. Wang, S. M. Kamali, E. Arbabi, A. Arbabi, Z. Zhao, G. Xie, Y. Cao, N. Ahmed, Y. Yan, C. Liu, A. J. Willner, S. Ashrafi, M. Tur, A. Faraon, and A. E. Willner, "Orbital angular momentum-based space division multiplexing for high-capacity underwater optical communications," Scientific Reports **6**, 33306 (2016).
18. L. Li, R. Zhang, Z. Zhao, G. Xie, P. Liao, K. Pang, H. Song, C. Liu, Y. Ren, G. Labroille, P. Jian, D. Starodubov, R. Bock, M. Tur, and A. E. Willner, "High-capacity free-space optical communications between a ground transmitter and a ground receiver via a UAV using multiplexing of multiple orbital-angular-momentum beams," Scientific Reports **7**, 17427 (2017).
19. L. Li, R. Zhang, P. Liao, Y. Cao, H. Song, Y. Zhao, J. Du, Z. Zhao, C. Liu, K. Pang, H. Song, D. Starodubov, B. Lynn, R. Bock, M. Tur, A. F. Molisch, and A. E. Willner, "MIMO equalization to mitigate turbulence in a 2-channel 40-Gbit/s QPSK free-space optical 100-m round-trip orbital-angular-momentum-multiplexed link between a ground station and a retro-reflecting UAV," In 2018 *European Conference on Optical Communication (ECOC)*, Th2.33 (2018).
20. G. Labroille, B. Denolle, P. Jian, P. Genevaux, N. Treps, and J.-F. Morizur, "Efficient and mode selective spatial mode multiplexer based on multi-plane light conversion," Optics Express **22**, 15599 (2014).
21. B. Rodenburg, M. P. J. Lavery, M. Malik, M. N. O'Sullivan, M. Mirhosseini, D. J. Robertson, M. Padgett, and R. W. Boyd, "Influence of atmospheric turbulence on states of light carrying orbital angular momentum," Optics Letters **37**, 3735-3737 (2012).
22. M. J. Padgett, F. M. Miatto, M. P. J. Lavery, A. Zeilinger, and R. W. Boyd, "Divergence of an orbital-angular-momentum-carrying beam upon propagation," New Journal of Physics **17**, 023011 (2015).
23. G. Xie, L. Li, Y. Ren, H. Huang, Y. Yan, N. Ahmed, Z. Zhao, M. P. J. Lavery, N. Ashrafi, S. Ashrafi, R. Bock, M. Tur, A. F. Molisch, and A. E. Willner, "Performance metrics and design considerations for a free-space optical orbital-angular-momentum multiplexed communication link," Optica **2**, 357-365 (2015).